Cationic and magnetic order in LiNiO$_2$- and NiO-type Li-Ni mixed oxides

C. B. Azzoni

Istituto Nazionale di Fisica della Materia, Dipartimento di Fisica "Alessandro Volta," Università degli Studi di Pavia,
via Bassi 6, I-27100 Pavia, Italy

A. Paleari

Istituto Nazionale di Fisica della Materia, Dipartimento di Fisica, Università degli Studi di Milano,
via Celoria 16, I-20133 Milano, Italy

V. Massarotti, M. Bini, and D. Capsoni

Dipartimento di Chimica-Fisica, Università degli Studi di Pavia, via Taramelli 16, I-27100 Pavia, Italy

X-ray diffraction, magnetic susceptibility, and electron paramagnetic resonance (EPR) measurements have been carried out on mixed nickel-lithium oxides as a function of the lithium content. The experimental results allow us to analyze the cationic order and the magnetic interactions. All the data are consistent with a model that admits coexistence of different structural phases in a wide composition range, previously not accounted for in the discussion of the physical properties of these mixed oxides.

I. INTRODUCTION

Two different kinds of solid solutions are present in the system NiO/Li$_2$O and their crystallographic structures are well described in the literature.[1–3]

(i) Substitutional solid solutions (SSS's) Li$_x$Ni$_{1-x}$O, of NiO-structure type (NaCl related), have a unique cationic site containing both lithium and nickel randomly distributed. The cubic NaCl-like cell can be rhombohedrally distorted (space group $R\bar{3}m$) for very low lithium content. Because of their semiconductive behavior, these materials are widely used in the preparation of devices for electrochemical cells.[4]

(ii) Ordered solid solutions (OSS's) Ni(Li$_{1-y}$Ni$_y$)O$_2$, usually reported as Li$_{2x}$Ni$_{2-2x}$O$_2$, are derived from the LiNiO$_2$ layered structure (space group $R\bar{3}m$). The order is due to the preferred occupation of the two cationic sites by different ions. These materials are used both in the preparation of the electrodes for Li batteries[5–8] and in the design of oxidation-selective catalysts.[9,10]

Samples with lithium cationic fraction x less than 0.31 are reported in the literature as SSS compounds, while the OSS phase is related to the compositions with $x > 0.31$.[2,3,9] The structural difference between LiNiO$_2$- and NiO-type solid solutions can be clearly explained on the basis of the cation layer sequence. The double hexagonal c parameter of the LiNiO$_2$ cell with respect to the NiO-like hexagonal cell is due to the presence of alternate cationic planes. The atomic layers represent the 001 families of planes relative to the hexagonal axes or the 111 planes for cubic lattice translation. The c hexagonal axis represents the diagonal of a multiple cubic cell. Stoichiometric LiNiO$_2$ is very difficult to prepare[1,2–4,11] and a small lithium deficiency, due to nickel atoms occupying lithium sites rather than to Li$^+$ ion vacancies, is almost unavoidable.

The magnetic properties of these materials are strongly affected by the composition and by the degree of cationic order.[1,12,13] In fact, the lithium substitution may result both in a dilution of the NiO antiferromagnetic phase (for low Li content) and in a ferrimagnetic phase reflecting the presence of two kinds of magnetic ions (Ni^{2+} and Ni^{3+}) in the cationic arrangement of the layered LiNiO$_2$-type structure. Low-temperature magnetic features observed in quasistoichiometric LiNiO$_2$ show that site-to-site inhomogeneities may also be found, giving rise to the typical disordered magnetic phases of spin glasses.[14]

In addition, the magnetic response is also related to the transport properties, depending on the degree of delocalization of the holes introduced by lithium substitution. Actually, complementary points of view are indeed reported as regards the charge and the spin changes locally created by lithium addition.[15] However, the nickel 3d character of the lithium-introduced holes, for high doping levels, seems now accepted.[16] A related open question regards the electron paramagnetic resonance (EPR) signal observed in OSS samples and attributed to low-spin Ni^{3+} ions ($S=1/2$),[1,12] even though strongly anisotropic spin states were also proposed.[17] Detailed studies of the thermal behavior of the EPR linewidth near the magnetic transition have also been carried out.[13]

The aim of the present work is to give a phenomenological assessment of the relations among bulk composition, structural cationic order, and magnetic phases, pointing out the crucial role of the preparation method before any detailed attribution of the magnetic features as a function of the lithium substitution. By comparing the results of x-ray-diffraction analysis, susceptibility and magnetization data, and EPR measurements, we show evidence of a possible equilibrium between different structural phases in a wide composition range, previously not accounted for in the discussion of the magnetic properties of these mixed oxides.

II. EXPERIMENTAL DETAILS

The samples investigated were prepared from the reactive system NiO/Li$_2$CO$_3$. The reagents were intimately mixed by
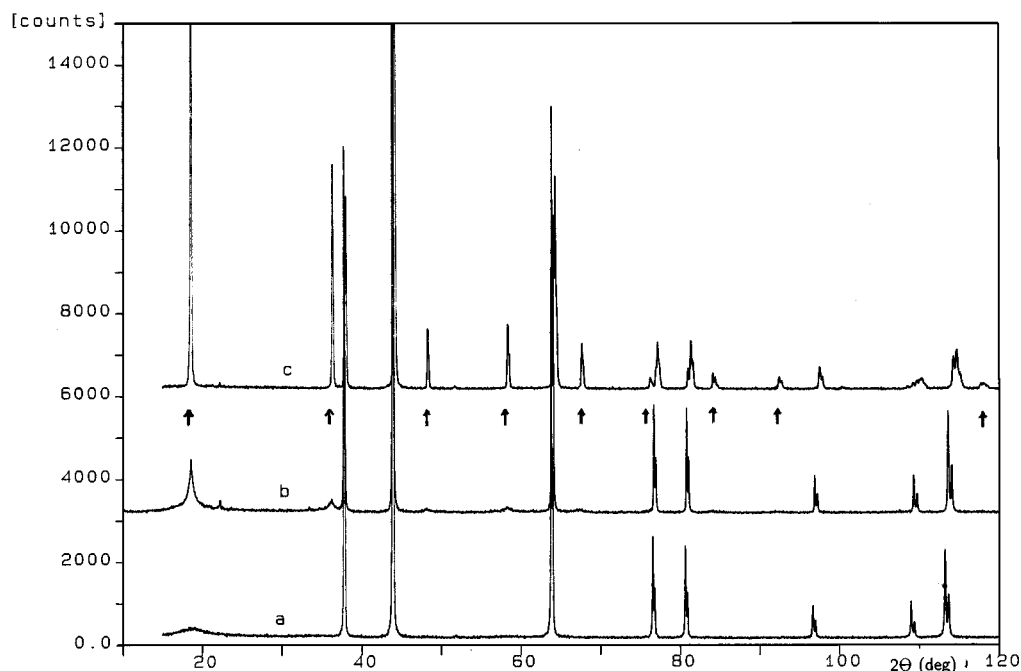
FIG. 1. X-ray-diffraction patterns of samples with (curve a) $x=0.20$, prepared by method B, (curve b) $x=0.26$ prepared by method A, and (curve c) $x=0.40$. The arrows indicate the double-cell reflections (see text).

grinding in an agate mortar and then heated at 5 °C/min up to 800 °C in alumina. An isothermal step at this temperature was held for the proper annealing time and then the samples were cooled at 5 °C/min to room temperature. Two sets of samples were prepared with $0.05 \leqslant x \leqslant 0.46$ by following two different methods.

(i) Method A: 0.5 initial lithium cationic fraction. Lower-lithium-content samples are obtained after very long annealing time by the decrease of lithium content due to Li_2O evaporation.[1]

(ii) Method B: the desired final composition was obtained by preserving the initial lithium content by short annealing times.

X-ray-diffraction (XRD) data were obtained with a Philips PW 1710 powder diffractometer equipped with a Philips PW 1050 vertical goniometer. Use was made of the Cu $K\alpha$ radiation obtained by means of a graphite monochromator. Patterns were collected in the angular range $15° < 2\theta < 150°$ in step scan mode with a step width of $0.03°$ and 1 s of counting time. Diffraction measurements were carried out from 300 down to 10 K using a Guinier-Huber diffractometer with a helium cooling device.

Static magnetic susceptibility measurements were carried out from 300 down to 77 K at a magnetic field of 50 mT by using a Faraday balance susceptometer with a sensitivity of 0.1 μg and a continuous-flow cryogenic apparatus. For sample masses of a few 10^{-2} g, the resulting sensitivity is about 10^{-7} cm^3/g. The error on the absolute mass susceptibility data, derived from the accuracy in the magnetic-field gradient value, is estimated to be less than 10%. The magnetic-field dependence of the magnetization was also monitored at different temperatures by changing the field intensity between 5 and 150 mT.

EPR spectra were detected in the temperature range 120–300 K by using a Bruker spectrometer at 9.12 GHz. The modulation field, the microwave power, and the sample position in the resonant cavity were kept constant for correct signal comparison. Care was taken to ensure thermal stabilization of the sample during spectra recording. Signal areas and spin densities were estimated by numerical analysis and by comparison with paramagnetic standards.

III. RESULTS

A. X-ray diffraction

In Fig. 1 the x-ray-diffraction patterns at room temperature of three samples are reported in the angular range $15° < 2\theta < 115°$. Pattern a refers to material with low lithium content ($x=0.20$) prepared by method B, pattern b to a sample prepared by method A and with $x=0.26$, while pattern c refers to a Li-rich $LiNiO_2$-like compound ($x=0.40$): with $x>0.31$, similar patterns are obtained from samples prepared by A and B methods. Two kinds of features turn out to change with the lithium content: the angular positions of the peaks belonging to the rhombohedrally distorted NiO-like structure, and the presence of additional peaks due to the layered OSS phase (indicated by arrows). This second feature is typical of samples with $x>0.31$ and of samples with $x<0.31$ if prepared by method A.

The angular shift of the peak position reflects the change of the a and c single-cell parameters, decreasing from 0.295 to 0.290 nm and from 0.721 to 0.712 nm, respectively, on increasing the lithium content from $x=0.05$ to 0.31. On the other hand, the additional peaks show the formation of a double-cell structure with $1.426>c>1.420$ nm and $0.290>a>0.288$ nm for the Li cationic fraction ranging between $x=0.31$ and 0.46.

X-ray-diffraction patterns were analyzed by the Rietveld refinement procedure[18,19] in order to obtain structural and

TABLE I. As a function of the total lithium content x and of the preparation method A or B (for the samples with $x<0.31$), the following parameters are reported: lattice constants a and b, OSS and SSS phase percentage, and, for each phase, x_{OSS} and x_{SSS} lithium contents deduced from XRD; percentages of OSS phase, lithium content x_{OSS}, transition temperature T_c, and α and γ coefficients (see text) deduced from the χ data; $d(\Delta B)/dT$, spin densities, and T_c values inferred from $\Delta B(T)$, resulting from EPR measurements.

x	0.461	0.416	0.399	0.359	0.314	0.257 A	0.201 A	0.196 B	0.181 B	0.105 B	0.045 B
					XRD data						
OSS											
a (nm)	0.2881	0.2889	0.2891	0.2896	0.2903	0.2908	0.2911				
c (nm)	1.4205	1.4222	1.4226	1.4237	1.4259	1.4266	1.4296				
% OSS	100.0	100.0	100.0	100.0	67.9	24.1	8.8				
x_{OSS}	0.461	0.416	0.399	0.359	0.348	0.308	0.268				
SSS											
a (nm)					0.2904	0.2909	0.2920	0.2918	0.2930	0.2940	0.2947
c (nm)					0.7121	0.7129	0.7143	0.7148	0.7174	0.7196	0.7213
% SSS					32.2	75.9	91.2	100.0	100.0	100.0	100.0
x_{SSS}					0.241	0.241	0.194	0.196	0.181	0.105	0.045
					χ data						
% OSS	100.00	100.00	100.00	100.00	67.00	25.00	9.00				
x_{OSS}	0.46	0.40	0.40	0.38	0.37	0.35	0.37				
T_c (K)		214	214	241	252	267	253				
α	492	570	569	596	599	572	599				
γ	224	670	668	671	669	684	670				
					EPR data						
T_c (K)		215	218	238	258	293	278				
$d(\Delta B)/dT$ (mT K^{-1})	0.64	1.45	1.44	2.00	2.20	2.56	2.37				
Spin density (10^{21} cm^{-3})	2.8	5.5	5.5	9.7	8.5	0.15	0.17				

profile parameters. This minimization procedure consists of a least-squares fit which uses an intensity function accounting for reflection contributions from one or more phases, besides the background component. Fits of the observed patterns were successfully obtained with single-phase and two-phase models from the following structures:

(i) SSS NiO type with a simple c-axis hexagonal cell (cationic site 0,0,0 and anionic site 0,0,1/2);

(ii) OSS LiNiO$_2$ type with double c-axis hexagonal cell [first cationic site (Ni) 0,0,0, second cationic site (Li,Ni) 0,0,1/2, and anionic site 0,0,z with $z\cong1/4$).

The percentage of each phase is deduced from the fit together with the lattice parameters a and c. The detailed procedure is described in Ref. 20. The results are shown in Table I, reporting, as a function of the total lithium content x, cell parameters, OSS and SSS phase percentage, and, for each phase, lithium content x_{OSS} and x_{SSS}.

We remark that the samples with $x>0.31$ consist of the OSS phase, while the samples with $x<0.31$, if produced by method B, consist of the SSS phase and, if produced by method A, are two-phase systems.

B. Susceptibility and magnetization

In Fig. 2 the temperature dependences of the mass susceptibility χ_m and of χ_m^{-1} are reported for three samples with high content of lithium ($x>0.31$), i.e., samples that show very strong double-cell features in the x-ray pattern (see Fig. 1, curve c).

Figure 2(a), concerning a sample with $x=0.46$ and comparable to a quasistoichiometric LiNiO$_2$ compound, shows a paramagnetic behavior, slightly deviating from the Curie-Weiss law at about 100 K. It is similar to that already observed in Ref. 12 and described by a high-temperature Curie-Weiss law typical of ferromagnets.[21]

Figures 2(b) and 2(c), concerning samples with $x=0.40$ and 0.36, respectively, show a change of behavior in the temperature range investigated, consisting in a rapid increase of the slope of χ_m around a critical temperature T_c. Similar features are found in samples with lithium cationic fraction $x<0.31$ when prepared by following the method A, as shown in Figs. 3(a) ($x=0.20$) and 3(b) ($x=0.26$). In the x-ray pattern, these samples also show double-cell features (marked by arrows in Fig. 1 curve b) even though detected together with intense reflection peaks typical of the single-cell phase.

Samples with $x<0.31$ but prepared according to the method B do not show any transition in the χ_m curve nor paramagnetic behavior [Fig. 3(c) with $x=0.20$] and their diffraction patterns do not possess the double-cell features as shown in Fig. 1 curve a. Their susceptibility is temperature independent, with values of a few 10^{-5} cm^3/g.

The magnetization data show that the observed abrupt variations of χ_m^{-1} are indeed related to a magnetic transition, as follows.

(i) The magnetization curves of samples with $x>0.31$ [see Fig. 4(a) for $x=0.40$] have linear paramagnetic behavior above T_c but lack linearity below it. We did not observe any change in x-ray pattern in the same temperature range suggesting a structural transition.
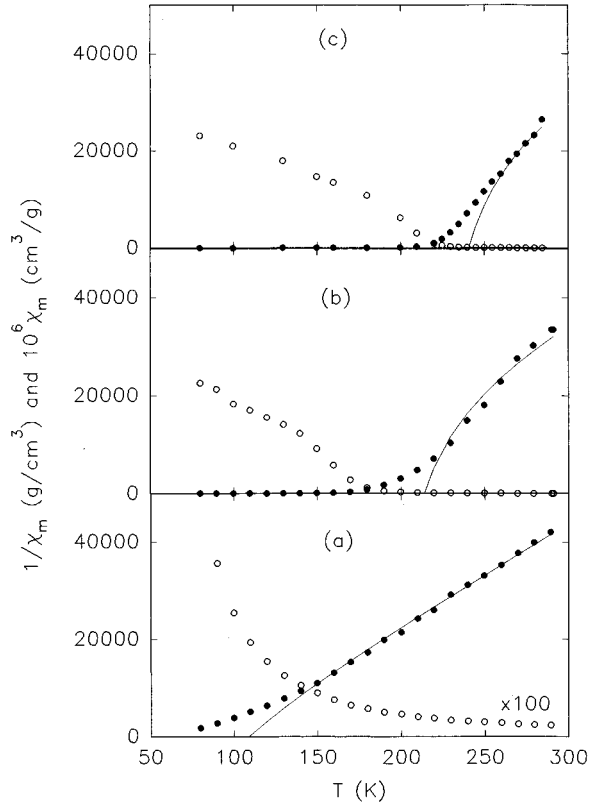
FIG. 2. Temperature dependence of the static magnetic mass susceptibility χ_m (open circles) and of χ_m^{-1} (filled circles) for samples with (a) $x=0.46$, (b) $x=0.40$, and (c) with $x=0.36$.

FIG. 3. Temperature dependence of the static magnetic mass susceptibility χ_m (open circles) and of χ_m^{-1} (filled circles) for samples with (a) $x=0.20$ and (b) $x=0.26$ both prepared by method A and (c) with $x=0.20$ prepared by method B.

(ii) Samples with $x<0.31$ and obtained by method A have magnetization curves similar to those of $x>0.31$ samples but with values an order of magnitude lower, as shown in Fig. 4(b) ($x=0.26$).

Samples with $x<0.31$ and prepared with method B show nonlinear magnetization in the investigated temperature range [Fig. 4(c) for $x=0.20$], according to a field-dependent low susceptibility.

C. EPR measurements

No relevant EPR signal is detected in samples with low content of lithium ($x<0.31$) and prepared with method B. On the other hand, a strongly temperature-dependent signal characterizes the samples showing a magnetic transition and double-cell peaks in the x-ray-diffraction pattern. At $T>T_c$ this signal is symmetric with g factor $\cong 2.139$ and very broad, as already observed.[13] It is narrowed by decreasing the temperature, down to a minimum linewidth ΔB observed near T_c: about this temperature it becomes asymmetric, begins to broaden and its area increases following the susceptibility behavior. Calculations of the spin density give typical values ranging between 10^{20} and 10^{22} cm^{-3}. Below T_c the signal splits into several components with resonant fields strongly dependent on the temperature: the number of these components is sample dependent.

IV. DISCUSSION

Comparisons between susceptibility, magnetization, and EPR data allow us to identify specific magnetic features per-

taining to the OSS LiNiO$_2$-type structure: the magnetic transition and the EPR signal. We observe that both the magnetic critical temperature T_c and the EPR signal narrowing above T_c turn out to be composition and structure dependent. Previous studies showed that a minimum critical value $x=0.31$ of lithium substitution is needed to stabilize the ordered layered structure. But we point out the crucial role of the synthesis process, which may give products with the same bulk composition but different physical properties. In fact, we observe the presence of magnetic transition and EPR signal also in materials with x less than 0.31 when prepared starting with excess of lithium. We interpret this result as evidence of the possible coexistence of OSS and SSS structures. We will show that the observed magnetic properties are consistent with the x-ray-diffraction model and, moreover, this agreement allows us to detail the structure of layered compounds as concerns the cationic and magnetic ordering.

A. Magnetic properties

The magnetization curve of Fig. 4(b) suggests a two-phase model: one observes an abrupt change of M by decreasing the temperature below T_c, as in typical lithium-rich samples [see Fig. 4(a)], but the M values are more than a factor of 10 smaller, approaching the values observed in antiferromagnetic low-Li-content samples [see Fig. 4(c)].

In order to test this model, the paramagnetic response of the samples must be analyzed in some detail. From the χ_m curves of the SSS samples, we may suppose that the disor-
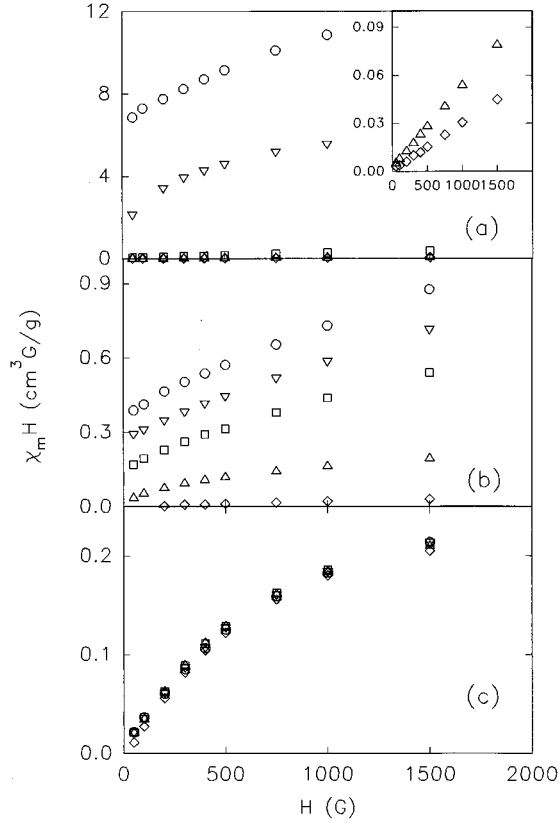
FIG. 4. Magnetization curves at 300 K (diamonds), 250 K (up triangles), 200 K (squares), 150 K (down triangles), and 100 K (circles) of samples (a) with $x=0.40$, (b) with $x=0.26$ prepared by method A, and (c) with $x=0.20$ prepared by method B.

dered phases give temperature-independent contributions to χ_m. As regards the OSS phases, we have to consider the existence of a superstructure of cationic planes containing Li$^+$ ions intercalated by planes of nickel without lithium. In addition, we suppose that the Ni^{3+} ions introduced by lithium substitution enter preferentially in the nickel planes, so as to progressively approach the cationic structure of the stoichiometric LiNiO₂. Really, this assumption just suggests a ferrimagnetic transition, implying the existence of some distinction between the cationic sites occupied by each species of magnetic ion (Ni^{2+} and Ni^{3+}), so as to give rise to uncompensated antiferromagnetically coupled sublattices. In fact, we have verified that, if the Ni^{3+} ions were randomly distributed, explicit mean-field calculations of the paramagnetic response above T_c would give rise to an average Curie-Weiss behavior without the hyperbolic divergence of χ_m^{-1} typical of a ferrimagnet.

Therefore we model the cationic arrangement in the OSS phase by alternating 001 planes in the hexagonal setting of Ni^{2+} and Ni^{3+} ions ["heavy" (H) planes] and of Ni^{2+} and Li$^+$ ions ["light" (L) planes], constituting a structure usefully described by the formula $[Li_{2x}^+Ni_{1-2x}^{2+}]_L[Ni_{1-2x}^{2+}Ni_{2x}^{3+}]_HO_2$.[11] The molar magnetization may thus be written as

$$M = 2xM_{Ha} + (1-2x)M_{Hb} + (1-2x)M_{Lb}, \quad (1)$$

where the subscripts H and L refer to the "heavy" only-nickel and "light" with-lithium planes, while a and b indicate contributions from Ni^{3+} and Ni^{2+}, respectively. Following the Van Vleck approach, the sublattice magnetizations may be expressed in terms of the local fields H_H and H_L:

$$M_{Ha} = C_aH_H/T,$$

$$M_{Hb} = C_bH_H/T,$$

$$M_{Lb} = C_bH_L/T, \quad (2)$$

with

$$C_a = \frac{N_A\mu_B^2}{3k_B}g_a^2J_a(J_a+1), \quad C_b = \frac{N_a\mu_B^2}{3k_B}g_b^2J_b(J_b+1).$$

N_A, μ_B, and k_B are the Avogadro number, the Bohr magneton, and the Boltzmann constant, while g and J may be approximated, respectively, by 2 and by the spin-only values of the Ni^{3+} ions, in low-spin configuration,[1,12,22] and of Ni^{2+} ions. The local magnetic interactions are accounted for by contributions to the local fields from the sublattice magnetizations weighted by ferromagnetic and antiferromagnetic α and γ interaction coefficients:

$$H_H = H - \gamma(1-2x)M_{Lb} + \alpha 2xM_{Ha} + \alpha(1-2x)M_{Hb},$$

$$H_L = H + \alpha(1-2x)M_{Lb} - \gamma 2xM_{Ha} - \gamma(1-2x)M_{Hb}. \quad (3)$$

By substituting in (3) the expressions for H_H and H_L given by the mean-field relations (2), one obtains three equations in M_{Ha}, M_{Hb}, and M_{Lb}. Solving the system, the molar susceptibility χ_M is written as $M(x,\alpha,\gamma,T)/H$, where M is calculated by using Eq. (1). The continuous lines in Figs. 2 and 3 are the results of fits calculated within this model: the data range for the fitting excludes the transition region, where the mean-field theory is unreliable.

From α and γ, the ferromagnetic intraplane and antiferromagnetic interplane exchange constants j' and j'' may be estimated. Since each magnetic ion has six neighboring ions in the same plane and three in the two adjacent ones, the mean-field coefficients from the sum of 12 exchange contributions averaged over the possible coordinations of Ni^{3+} and Ni^{2+} ions for the given lithium composition are

$$\alpha = \left\langle \sum_1^6 j'/C_i \right\rangle, \quad \gamma = -\left\langle \sum_1^6 j''/C_i \right\rangle, \quad (4)$$

where C_i may be C_a or C_b depending on the specific ion considered (Ni^{3+} or Ni^{2+}, respectively). By substituting the averaged sums by sums of the C_i^{-1} terms weighted by the presence of Ni^{3+} or Ni^{2+}, we finally obtain the expressions of j' and j'' as a function of α, γ, and x:

$$j' = \frac{\alpha}{6}\left(\frac{2x}{C_a} + \frac{1-2x}{C_b}\right)^{-1}, \quad j'' = -\frac{\gamma}{6}\left(\frac{x}{C_a} + \frac{1-x}{C_b}\right)^{-1}. \quad (5)$$

The j' and j'' exchange constants so estimated for the samples with OSS features ($x=0.46$ excluded) fall into narrow ranges, j' being 43 ± 2 K, and j'' -70 ± 2 K. The j''

values well match the exchange constant $j''=-85$ K of the parent compound NiO.[23] In fact, in both cases, the intersublattice interactions are mediated by the same type of exchange geometry, though the magnetic structure is completely different (fcc in NiO and layered in OSS $Li_{2x}Ni_{2-2x}O_2$). This latter fact is just the reason, by contrast, that the estimated j' cannot be compared with the value reported for NiO [$j'(NiO)=-55$ K] since the intrasublattice interactions have very different features.

The calculated j' and j'' for the "quasistoichiometric" sample with $x=0.46$ deviate from the values observed in the other OSS compounds, giving $j'=32$ K and $j''=-21$ K. This result agrees with the prevalence of ferromagnetic intralayer interactions[12] expected on approaching the $LiNiO_2$ structure where the interlayer interactions are quenched by the diamagnetic lithium layers. The lower value of the ferromagnetic j' constant might be related to less efficient intralayer exchange interactions when the number of Ni^{2+} ions in the heavy layers becomes very small. This result calls for further investigation[21] about the effects of the coexistence of Ni^{2+} and Ni^{3+} on the intralayer ferromagnetic exchange interactions.

The percentages of OSS phase and the lithium contents x_{OSS} resulting from this approach are reported in Table I for comparison with the analogous data from diffraction analysis: the agreement between the percentages of OSS phase and the similar trends of x_{OSS} is remarkable and supports in a nontrivial way the coexistence of the two different SSS and OSS structures.

B. EPR data

The comparison between the EPR spectra of samples in a wide composition range brings us to the definite association of the EPR signal with the OSS layered structure.
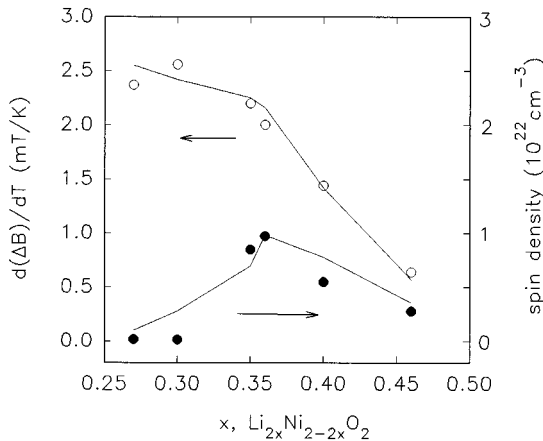
FIG. 5. (Open circles) linear thermal dependence coefficient $d(\Delta B)/dT$ of the EPR linewidth. (Filled circles) spin density estimated from the EPR signal area. The data are reported according to the x value of the only-OSS phase. The upper continuous line is the experimental curve obtained by Stoyanova, Zhecheva, and Friebel (Ref. 24). The lower line is the expected statistical abundance of facing Ni^{3+}-O-Ni^{2+} couples.

The large area of the signal points to a "bulk" attribution, ruling out the defect sites as origin. In fact, by comparing the signal areas with the expected abundance of Ni^{3+} and Ni^{2+} ions for a given lithium addition, we find agreement with the density of 180°-faced Ni^{3+}-O-Ni^{2+} groups as already suggested.[13] In Fig. 5 we report the spin density, estimated from the EPR signal areas, compared with the Ni^{3+}-O-Ni^{2+} abundance (normalized to the largest density observed), calculated according to the relative occupation probabilities of Ni^{3+} and Ni^{2+} in adjacent cationic H and L planes:

$$P(Ni_H^{3+}\text{-O-}Ni_L^{2+})=P(Ni_H^{3+})P(Ni_L^{2+})=2x(1-2x). \quad (6)$$

The experimental points well match the ones calculated by assuming the x values of the OSS phase deduced from the x-ray-diffraction and susceptibility analyses within the two-phase model.

The linewidth thermal behavior is the other x-dependent feature in the EPR spectra. We calculated the slope $d(\Delta B)/dT$ of the EPR signal narrowing above T_c. This parameter was previously related[24] to "stoichiometry-dependent phonon modulation of the line broadening due to dipole-dipole interactions" in OSS compounds with $x>0.31$: in fact, a good reproduction of the experimental data observed in single-phase compounds was achieved. In Fig. 5 we also report our $d(\Delta B)/dT$ values, taking into account the OSS compositions reported in Table I. We remark that the data for two-phase samples with $x<0.31$ prepared with method A also well match the other data.

In a few samples (such as that with $x=0.40$ of Figs. 2, 4, and 5) the slope $d(\Delta B)/dT$ is not strictly constant but shows a slight decrease near the magnetic transition which also appears rather smooth in the χ_m^{-1} curve. This fact is likely due to the presence of a variety of OSS regions with slightly different compositions, confirming that inhomogeneities may be easily found in these materials, as already observed in the "quasistoichiometric" compound.[14]

In Table I, besides $d(\Delta B)/dT$ and the spin densities, the T_c values inferred from $\Delta B(T)$ are reported for comparison with the T_c values resulting from the mean-field approach.

V. SUMMARY

Our results contribute to clarification of the relation between magnetic and structural features in these mixed oxides and indicate the importance of the preparation method, which may allow the coexistence of SSS and OSS structures with different lithium content, for samples prepared with very long annealing time and low final lithium content ($x<0.31$). In such cases one can expect some inhomogeneity between the surface and the inner part of the grains. However, the magnetic properties have been interpreted, in a simple mean-field approach, as a result of diluted antiferromagnetic contributions from the SSS phase and ferrimagnetic behavior of the OSS phase with T_c dependent on the phase composition. In summary, we have verified that the magnetic properties of the mixed Li-Ni oxide solutions are strictly related to the cationic arrangement within the lattice, and a model has also been proposed for the ordering of the differently charged nickel ions.

[1] J. B. Goodenough, D. G. Wickham, and W. J. Croft, J. Phys. Chem. Solids **5**, 107 (1958).

[2] W. Li, J. N. Reimers, and J. R. Dahn, Phys. Rev. B. **46**, 3236 (1992).

[3] J. N. Reimers, W. Li, and J. R. Dahn, Phys. Rev. B. **47**, 8486 (1993).

[4] *Molten Carbonate Fuel Cell Technology*, edited by J. R. Selman and T. D. Claar (Electrochemical Society, Pennington, NJ, 1982).

[5] T. A. Hewston and B. L. Chamberland, J. Phys. Chem. Solids **48**, 97 (1987).

[6] M. M. Thackeray, L. A. De Picciotto, W. I. F. David, P. G. Bruce, and J. B. Goodenough, J. Solid State Chem. **67**, 285 (1987).

[7] J. R. Dahn, U. Von Sacken, and C. A. Michal, Solid State Ionics **44**, 87 (1990).

[8] T. Ohzuku, A. Ueda, and M. Nagayama, J. Electrochem. Soc. **140**, 1862 (1993).

[9] I. J. Pickering, J. T. Lewandowski, A. J. Jacobson, and J. A. Goldstone, Solid State Ionics **53−56**, 405 (1992).

[10] M. Hatano and K. Otsuka, J. Chem. Soc. Faraday Trans. 1 **85**, 199 (1989).

[11] G. Dutta, A. Manthiram, J. B. Goodenough, and J. C. Grenier, J. Solid State Chem. **96**, 123 (1992).

[12] J. P. Kemp, P. A. Cox, and J. W. Hodby, J. Phys. Condens. Matter **2**, 6699 (1990).

[13] R. Stoyanova, E. Zhecheva, and S. Angelov, Solid State Ionics **59**, 17 (1993).

[14] J. N. Reimers, J. R. Dahn, J. E. Greedan, C. V. Stager, G. Liu, I. Davidson, and U. Von Sacken, J. Solid State Chem. **102**, 542 (1993).

[15] P. Kuiper, G. Kruizinga, J. Ghijsen, G. A. Sawatzky, and H. Verweij, Phys. Rev. Lett. **62**, 221 (1989).

[16] M. A. van Veenendaal and G. A. Sawatzky, Phys. Rev. B **50**, 11 326 (1994).

[17] I. Yamada, K. Ubukoshi, and K. Hirakawa, J. Phys. Soc. Jpn. **54**, 3571 (1985).

[18] H. M. Rietveld, J. Appl. Crystallogr. **2**, 65 (1969).

[19] D. B. Wiles and R. A. Young, J. Appl. Crystallogr. **14**, 149 (1981).

[20] V. Massarotti, D. Capsoni, and M. Bini, Z. Naturforsch. Teil A **50**, 155 (1995).

[21] P. Ganguly, V. Ramaswamy, I. S. Mulla, R. F. Shinde, P. P. Bakare, S. Ganapathy, P. R. Rajamohanan, and N. V. K. Prakash, Phys. Rev. B **46**, 11 595 (1992).

[22] R. Stoyanova, E. Zhecheva, and C. Friebel, J. Phys. Chem. Solids **54**, 9 (1993).

[23] J. S. Smart, in *Magnetism*, edited by G. T. Rado and H. Sohl (Academic, New York, 1963).

[24] R. Stoyanova, E. Zhecheva, and C. Friebel, Solid State Ionics **73**, 1 (1994).